Nuclear Instruments and Methods in Physics Research A 598 (2009) 710–721

Contents lists available at ScienceDirect

Nuclear Instruments and Methods in Physics Research A

journal homepage: www.elsevier.com/locate/nima

Dual-Readout calorimetry with crystal calorimeters

N. Akchurin [a], M. Alwarawrah [a], A. Cardini [b], G. Ciapetti [c], R. Ferrari [d], S. Franchino [d], M. Fraternali [d], G. Gaudio [d], J. Hauptman [e], F. Lacava [c], L. La Rotonda [f], M. Livan [d], E. Meoni [f], D. Pinci [c], A. Policicchio [f], S. Popescu [a], G. Susinno [f], Y. Roh [a], W. Vandelli [g], T. Venturelli [f], C. Voena [c], I. Volobouev [a], R. Wigmans [a,*]

[a] Texas Tech University, Lubbock (TX), USA
[b] Dipartimento di Fisica, Università di Cagliari and INFN Sezione di Cagliari, Italy
[c] Dipartimento di Fisica, Università di Roma "La Sapienza" and INFN Sezione di Roma, Italy
[d] Dipartimento di Fisica Nucleare e Teorica, Università di Pavia and INFN Sezione di Pavia, Italy
[e] Iowa State University, Ames (IA), USA
[f] Dipartimento di Fisica, Università della Calabria and INFN Cosenza, Italy
[g] CERN, Genève, Switzerland

ARTICLE INFO

Article history:
Received 3 September 2008
Received in revised form
1 October 2008
Accepted 9 October 2008
Available online 1 November 2008

Keywords:
Calorimetry
Cherenkov light
Crystals
Optical fibers

ABSTRACT

The hadronic performance of a Dual-Readout calorimeter consisting of a crystal em section and a hadronic section read out with two types of optical fibers is studied with 200 GeV π^+. The em fraction of hadronic showers developing in this calorimeter system is determined event by event from the relative amounts of Cherenkov light and scintillation light produced in the shower development. Data are presented for two types of crystals ($PbWO_4$ and BGO), each of which offers unique opportunities in this respect. The information obtained with this technique may lead to an important improvement in the hadronic calorimeter performance.

1. Introduction

In many modern particle physics experiments, the calorimeter systems are primarily designed to meet performance requirements for the detection of electron and γ showers. The choices made to achieve this may turn out to have detrimental consequences for the quality of hadronic shower detection [1].

In recent years, a promising new technique has been developed, which is not subject to the limitations (e.g., a small sampling fraction) traditionally required for excellent hadron calorimetry: the Dual REAdout Method (DREAM). DREAM calorimeters are based on a simultaneous measurement of different types of signals which provide complementary information about details of the shower development. The first calorimeter of this type was based on a copper absorber structure, equipped with two types of active media. In this detector, scintillating fibers measured the total energy deposited by the shower particles, while Cherenkov light, generated by the charged, relativistic shower particles, was produced in undoped optical fibers. Since the shower particles generating Cherenkov light are almost exclusively found in the em shower component (dominated by π^0s produced in hadronic showers), a comparison of the two signals made it possible to measure the energy fraction carried by this component, f_{em}, event by event. As a result, the effects of fluctuations in this component, which are responsible for all traditional problems in non-compensating calorimeters, could be eliminated, and the hadronic shower energy was correctly reconstructed based on the electron calibration and the two measured hadronic signals. This led to an important improvement in the hadronic calorimeter performance [2–4].

In a recent paper [5], we have demonstrated that the same technique, and the advantages it offers for hadron calorimetry, can in principle also be applied to homogeneous calorimeters, whose signals are a mixture of scintillation and Cherenkov light. The improvement of the calorimeter performance is in that case determined by the precision with which the relative contributions of these two types of light to the total signal can be determined. This precision was limited by the fact that we used a very small ($<5\%$) forward/backward asymmetry to determine these contributions. Yet, the applicability of the principle was clearly established for the lead tungstate ($PbWO_4$) crystals used in these experiments. However, the fact that the crystals had to be oriented at an angle of 63° (i.e., the Cherenkov angle, θ_C) with respect to the direction of the incoming particles in order to

*Corresponding author. Tel.: +1 806 742 3779; fax: +1 806 742 1182.
E-mail address: wigmans@ttu.edu (R. Wigmans).

0168-9002/$ - see front matter © 2007 Elsevier B.V. All rights reserved.
doi:10.1016/j.nima.2008.10.010

observe the mentioned asymmetry means that this method cannot be used in a realistic 4π experiment.

In the present paper, we describe follow-up measurements that were performed with the goal of improving the above results in $PbWO_4$. In these measurements, we rely on differences in the time structure of the signals, rather than on the directionality of the light. This time structure was measured with a high-resolution (2.5 GHz) sampling oscilloscope. We also did measurements with another type of crystal (BGO), which offers additional advantages compared to $PbWO_4$. Even though Cherenkov light represents a much smaller fraction of the total BGO signal, it is easier to recognize because of large differences in the optical spectra and time structure.

In Section 2, we describe the detectors and the experimental setup in which they were tested. In Section 3, we discuss the experimental data that were taken and the methods used to analyze these data. The experimental results obtained with a single BGO crystal and with the $PbWO_4$ 19-crystal matrix are presented in Sections 4 and 5, respectively. A brief summary and conclusions are given in Section 6.

2. Detectors and experimental setup

2.1. Detectors and readout

The calorimeter system used in these experiments consisted of two sections. The electromagnetic section (ECAL) consisted of scintillating crystals, and the hadronic section was the original DREAM fiber calorimeter [2–4].

During one series of experiments, an ECAL consisting of 19 lead tungstate ($PbWO_4$) crystals was used.[1] Each crystal was 18 cm long, with a cross-section of $2.2 \times 2.2\,cm^2$. These crystals were arranged in a matrix, as shown in Fig. 1.

The crystals were not optically isolated from each other, and the light produced by showering particles was read out by only two photomultiplier tubes (PMTs), one located at each end of the crystal matrix, as indicated by the circle in Fig. 1. For the purpose of these tests, this ensemble of crystals was considered one unit. The PMTs were specially selected for this application, for which we needed a light detector that was fast, had a large surface area and a low gain. This unusual combination of properties was found in XP4362B,[2] a 6-stage PMT (nominal gain 10^4) with a 3-in. active surface area and a nominal rise time of 2.0 ns.

In another series of experiments, we used a single crystal of $Bi_4Ge_3O_{12}$ (BGO) as an electromagnetic calorimeter, placed upstream of the DREAM fiber calorimeter. This 24 cm long crystal was tapered, with a front face[3] of $2.4 \times 2.4\,cm^2$ and a rear face of $3.2 \times 3.2\,cm^2$. This crystal was read out with PMTs[4] from both ends. In between each crystal face and the PMT, an optical filter was mounted. For the smaller (front) face, a yellow filter (Y) was used, while the light exiting through the larger (rear) face had to pass through an ultraviolet (UV) filter.[5] The reasons for this arrangement are explained in Section 4.

The basic element of the hadronic DREAM calorimeter section was an extruded copper rod, 2 m long and $4 \times 4\,mm^2$ in cross-section. This rod was hollow, and the central cylinder had a diameter of 2.5 mm. Seven optical fibers were inserted in this hole. Three of these were plastic scintillating fibers, the other four fibers were undoped, intended for detecting Cherenkov light. The instrumented volume had a length of 2.0 m ($10\lambda_{int}, 100X_0$), an effective radius of 16.2 cm and a mass of 1030 kg. The fibers were grouped to form 19 hexagonal towers. The effective radius of each tower was 37.1 mm ($1.82\rho_M$). A central tower was surrounded by two hexagonal rings. The towers were longitudinally unsegmented. The fibers sticking out at the rear end of this structure were separated into 38 bunches: 19 bunches of scintillating fibers and 19 bunches of Cherenkov fibers. In this way, the readout structure was established. Each bunch was coupled through a 2 mm air gap to a PMT.[6]

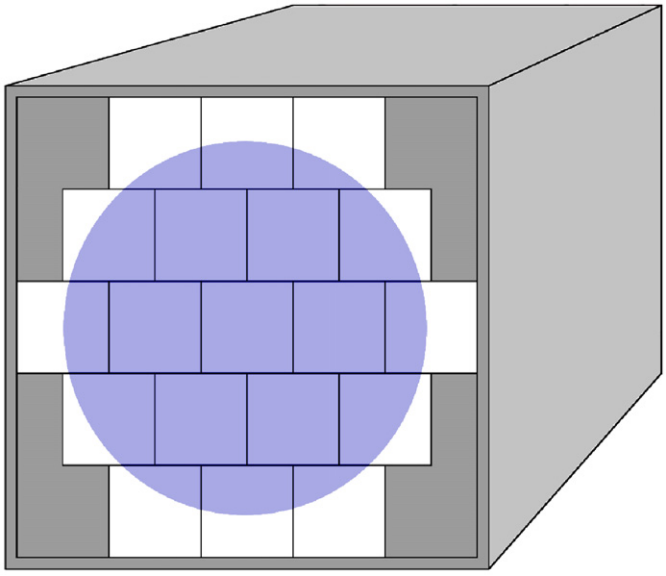

Fig. 1. The matrix of 19 $PbWO_4$ crystals that served as the em section of the calorimeter system. The circle indicates the size and the positioning of the PMTs used to detect the light generated in this matrix.

Extensive tests of this hadronic calorimeter module have shown that the combined information on the scintillation (S) and Cherenkov (C) light generated by hadronic showers made it possible to measure the em shower fraction event by event. As a result, this detector provided the same advantages as compensating calorimeters, despite e/h values of 1.3 and 4.7 for the S and C readout structures, respectively: a Gaussian response function, hadronic signal linearity, an energy resolution[7] that scales with $E^{-1/2}$ and, most importantly, correct reconstruction of the hadronic shower energy based on a calibration with electrons. Detailed information about this detector, and about the mentioned performance in stand-alone mode, is given in Refs. [2,3].

2.2. Experimental setup

All measurements described in this paper were performed in the H4 beam line of the Super Proton Synchrotron at CERN. The calorimeters were mounted on a platform that could move vertically and sideways with respect to the beam. Two small scintillation counters (TC) provided the signals that were used to trigger the data acquisition system. These trigger counters were 2.5 mm thick, and the area of overlap was $6 \times 6\,cm^2$. A coincidence

[1] On loan from the ALICE Collaboration, who use these crystals for their PHOS calorimeter.

[2] Manufactured by Photonis, France.

[3] The terms "front" and "rear" refer to the orientation of the crystal in the experimental setup (Fig. 3).

[4] Hamamatsu R1355, square (28 mm), 10-stage, with a $25 \times 25\,mm^2$ bialkali photocathode.

[5] Schott UG11 (UV) and GG495 (yellow). Filter thickness 3 mm.

[6] Hamamatsu R580, 10-stage, ϕ 38 mm, bialkali photocathode, borosilicate window.

[7] $\sigma/E = 64\%/\sqrt{E} + 0.6\%$ for 50–300 GeV jets, dominated by leakage fluctuations.

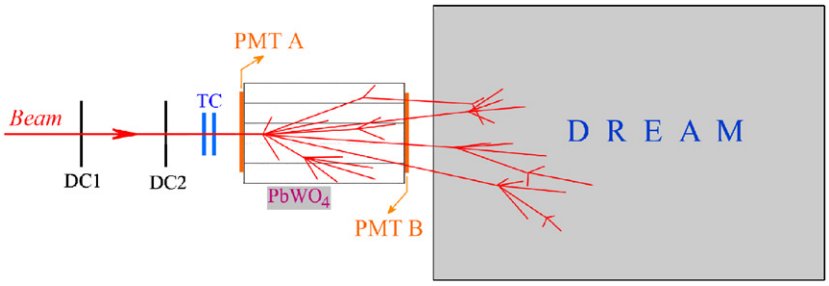

Fig. 2. Schematic (not to scale) of the experimental setup in which the $PbWO_4$ crystal matrix was tested in conjunction with the DREAM fiber calorimeter. Not shown is a $50 \times 50\,cm^2$ scintillation counter placed 8 m downstream of the DREAM calorimeter behind a 80 cm thick concrete block, which served as a muon counter.

between the logic signals from these counters provided the trigger. The trajectories of individual beam particles could be reconstructed with the information provided by two small drift chambers (DC1, DC2) which were installed upstream of the trigger counters. This system made it possible to determine the location of the impact point of the beam particles at the calorimeter with a precision of typically ~0.2 mm.

These and other aspects of the experimental setup used for the tests involving the $PbWO_4$ matrix are illustrated in Fig. 2. The crystal matrix was oriented such that the crystal axes were parallel to the beam direction (see also Fig. 1). In this way, this em calorimeter represented an absorber with an effective depth of $\approx 20X_0$. The two PMTs used to detect the light produced in the crystals will be called PMT A and PMT B, respectively.

The experimental setup used for the tests involving the BGO crystal is schematically shown in Fig. 3. The crystal axis coincided with the beam line, so that the 24 cm long crystal represented an em calorimeter with a depth of $\approx 21X_0$. The crystal was oriented as shown, with the yellow filter (Y) located upstream and the UV filter downstream. Because of the much larger light yield (compared to the $PbWO_4$ ECAL), combined with the higher PMT gain, it was necessary to limit the rate of the beam particles to about 1 kHz in these tests. The much higher rates that were easily available in this beam line led to non-linearities resulting from excessive anode currents. Because of the small cross-section of the crystals (even em showers experienced more than 20% lateral energy leakage in the BGO crystal), it was not deemed useful to use an upstream interaction target for these measurements. Fig. 3 shows the type of event studied here: a hadron starting a shower inside the BGO crystal, whose energy is shared with the DREAM detector. Since the interaction length of the crystal was slightly more than $1\lambda_{int}$, the majority of the beam hadrons were indeed of this type.

2.3. Data acquisition

Measurement of the time structure of the calorimeter signals formed a very important part of the tests described here. In order to limit distortion of this structure as much as possible, we used special 15 mm thick cables to transport the crystal signals to the counting room. Such cables were also used for the signals from the trigger counters, and these were routed such as to minimize delays in the DAQ system.[8] The HCAL signals were transported through RG-58 cables with (for timing purposes) appropriate lengths to the counting room. The crystal signals were sent into a unity-gain Linear Fan-out unit, output signals of which were used to measure the time structure and the total charge.

The data acquisition system used VME electronics. A single VME crate hosted all the needed readout and control boards. The charge measurements of the calorimetric signals from the crystals and the DREAM towers were performed with 2 CAEN V792AC QADC 32-channel modules,[9] each channel offering 12-bit digitization at a sensitivity of 100 fC/count and a conversion time below 10 μs. The signals from the muon counter were integrated and digitized with a sensitivity of 100 fC/count, on a 12-bit LeCroy 1182 module.[10] The timing information of the tracking chambers was recorded with 1 ns resolution in a 16-bit 16-channel LeCroy 1176 TDC.[11]

The time structure of the calorimeter signals was recorded by means of a Tektronix TDS 7254B digital oscilloscope,[12] which provided a sampling capability of 5 GSample/s, at an analog bandwidth of 2.5 GHz, over four input channels. During most of the data taking period only two channels were sampled, i.e., from the two PMTs reading out both sides of the crystal (matrix). The oscilloscope gain (scale) was tuned in order to optimize the exploitation of the 8-bit dynamic range, maintaining both a good sensitivity and a small fraction of overflow events.

The $PbWO_4$ signals were measured over a time interval of 112 ns, during which time 282 data points were collected. The BGO signals, which had a considerably longer decay time, were followed over a time interval that was twice as long, and measurements were performed every 0.8 ns. The quality of the information obtained in this way is illustrated in Fig. 4, which shows the average time structure of the signals from a pion crossing a single $PbWO_4$ crystal perpendicularly. As will be shown in Section 5, this excellent time resolution made it possible to distinguish the prompt Cherenkov peak from the fast decay component (<10 ns) of the $PbWO_4$ scintillation light.

The trigger logic was implemented through NIM modules and the signals sent to a VME I/O register, which was also catching the spill and the global busy information. Moreover, the system was able to inject pedestal triggers during the data taking, enabling the parallel recording of pedestal data. Pedestal events were flagged with a special signal on VME I/O register. The VME crate was linked to a data acquisition computer through an SBS 620 optical VME-PCI interface[13] that allows memory mapping of the VME resources via an open source driver.[14] The computer was equipped with a Pentium-4 2 GHz CPU, 1 GB of RAM, and running a CERN SLC 4.3 operating system.[15]

The data acquisition was built around a single-event polling mechanism and performed by a readout program that was streaming physics and on-spill pedestal events into two indepen-

[8] We measured the signal speed to be 0.78*c* in these cables.

[9] http://www.caen.it/nuclear/Printable/data_sheet.php?mod=V792&fam=vme&fun=qdc

[10] http://lecroy.com/lrs/dsheets/1182.htm

[11] http://www.lecroy.com/lrs/dsheets/1176.htm

[12] http://www.tek.com/site/ps/0,,55-13766-SPECS_EN,00.html

[13] http://www.gefanucembedded.com/products/457

[14] http://www.awa.tohoku.ac.jp/~sanshiro/kinoko-e/vmedrv/

[15] http://linux.web.cern.ch/linux/scientific4/

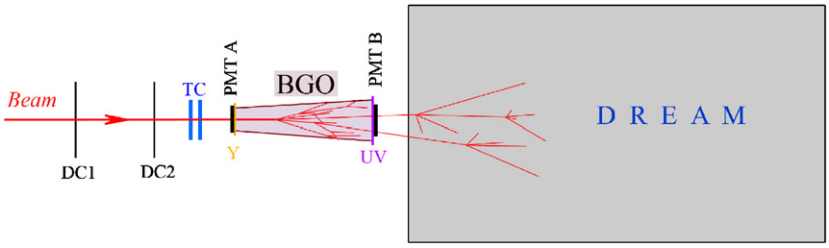

Fig. 3. Schematic (not to scale) of the experimental setup in which the BGO crystal was tested in conjunction with the DREAM fiber calorimeter. Not shown is a $50 \times 50\,cm^2$ scintillation counter placed 8 m downstream of the DREAM calorimeter behind a 80 cm thick concrete block, which served as a muon counter.

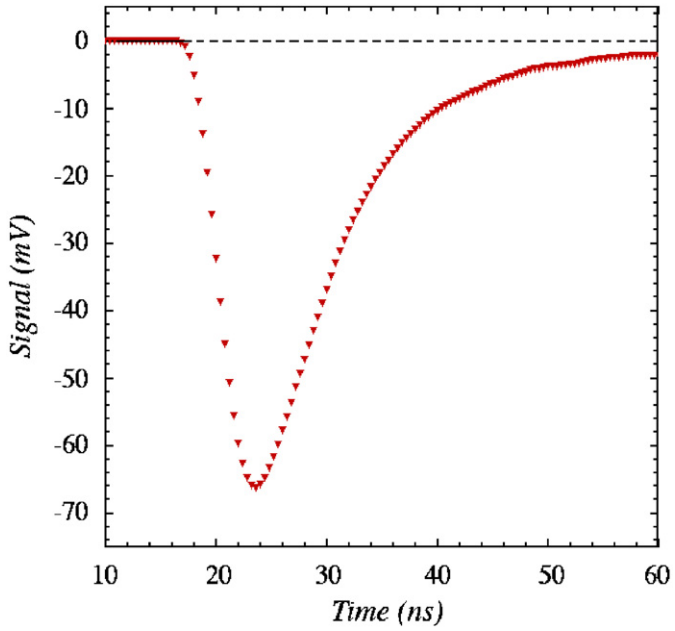

Fig. 4. Average time structure of the signals from a pion crossing a single lead tungstate crystal perpendicularly. The rise time of the signal (from 10% to 90% of the amplitude in 3.5 ns) is determined by the PMT and by the long cables (23 m) which transport the signals from the crystal to the oscilloscope, the trailing edge is determined by the $PbWO_4$ decay characteristics, with a dominating component of 10 ns [5].

dent first-in-first-out buffers, built on top of 32 MB shared memories. Two recorder programs were then dumping the data from the shared memories to the disk. Only exclusive accesses to shared buffers were allowed and concurrent requests were synchronized with semaphores. This scheme optimized the CPU utilization and increased the data taking efficiency thanks to the bunch structure of the SPS cycle, where beam particles were provided to our experiment during a spill of 4.8 s, with a repetition period of 16.8 s.

On the other hand, due to the large oscilloscope data size and its poor on-line performance, we decided to handle it on a multi-event basis. Through the GPIB interface, the digital scope was prepared to acquire events before the extraction and delivery of protons on target. On spill, all events were sequentially recorded in the internal memory of the scope. At the end of the spill, the oscilloscope memory was dumped over a temporary file, in a network-mounted shared disk. At this point, the file was read out and the data copied in properly formatted areas in the shared-memory buffers, where the information from all the VME modules had already been stored, in real time, by the readout program. In sequence, the recorder programs were then dumping the events to disk and a monitoring program was running in spy mode, on top of the physics shared memory, producing online histograms.

With this scheme, we were able to reach, in spill, a data acquisition rate of ~2 kHz, limited by the size of the internal scope buffer. Since no pedestal suppression was implemented, the data volume was proportional to this rate, and amounted, at maximum, to ~1.5 MB/spill, largely dominated by the oscilloscope data.

2.4. Calibration of the detectors

All PMTs used in these measurements were calibrated with 50 GeV electrons. The two PMTs reading out the two sides of the $PbWO_4$ crystal matrix were calibrated with the detector oriented as shown in Fig. 2. The PMTs reading out the BGO crystals were calibrated with the crystal oriented as shown in Fig. 3, and the filters in place. In both cases, longitudinal shower containment was adequate. However, lateral shower leakage was substantial in the case of BGO. According to our Monte Carlo simulations, the BGO crystal detected, on average, only 38.2 GeV of the energy carried by the beam electrons. The $PbWO_4$ matrix contained, on average, 47.3 GeV.

The 38 PMTs reading out the 19 towers of the HCAL were also all calibrated with 50 GeV electrons. The showers generated by these particles were not completely contained in a single calorimeter tower. The (average) containment was again found from EGS4 Monte Carlo simulations. When the electrons entered a tower in its geometrical center, on average 92.5% of the scintillation light and 93.6% of the Cherenkov light was generated in that tower [2]. The remaining fraction of the light was shared by the surrounding towers. The signals observed in the exposed tower thus corresponded to an energy deposit of 46.3 GeV in the case of the scintillating fibers and of 46.8 GeV for the Cherenkov fibers.

The mentioned energies, together with the precisely measured values of the average signals from the exposed crystals or calorimeter towers, formed the basis for determining the calibration constants, i.e., the relationship between the measured number of ADC counts and the corresponding energy deposit.

3. Experimental data and methods

The purpose of these tests was to split the crystal signals into their scintillation and Cherenkov components, and to see to what extent this event-by-event information could be used to improve the hadronic calorimeter performance of a calorimeter system of which these crystals formed the electromagnetic section.

3.1. Experimental data

All measurements were performed with 200 GeV π^+ beams. We collected 7×10^5 events for $PbWO_4$ and 1.6×10^6 events for

BGO. For each event, the time structure of both ECAL signals was measured (with 0.4 ns resolution in the case of $PbWO_4$, 0.8 ns for BGO). The integrated charge carried by these signals and by those from the 38 HCAL channels was digitized with 12-bit resolution. The pion beams contained some muons, at the few-% level. These muons were easily recognized (using the muon counter) and removed from the event samples. For reasons explained below, the signals from the UV side of the BGO crystal consisted of two distinctly different components. The signals from these components were separately digitized, using two different outputs of the Linear Fan-out.

3.2. Exploiting the BGO signals

The time structure of the signals from the BGO crystal observed with the yellow filter and the UV filter were very different [6].

This is illustrated in Fig. 5, which shows the time structures measured from both sides of the crystal (i.e., with the two different filters) for a typical shower developing in it. The scintillation spectrum of BGO is centered around a wavelength of 480 nm, i.e., in the yellow/green domain. The decay time of the scintillation process is ~300 ns. The yellow filter is highly transparent for this type of light, as reflected by the signal shape in Fig. 5a.

The UV filter is transparent for light in the wavelength region from 250 to 400 nm, which harbors a large fraction of the Cherenkov light, and little of the scintillation light. The time structure of the signals from the PMT placed behind the UV filter (Fig. 5b) clearly exhibits these two components. The (prompt) Cherenkov component is represented by the sharp peak, whereas the long tail has the same characteristic time structure as the pure scintillation signals generated by the light transmitted through the yellow filter.

The signals from the PMT that detects the light transmitted through the UV filter thus contains event-by-event information about the relative contributions of Cherenkov and scintillation photons. We have taken advantage of this feature by generating digitized signals for both components.

Output signals from the Linear Fan-Out were used to generate two ADC gates, which corresponded to different time intervals (Fig. 6). Gate 1 was used to digitize the part of the signals that contained the Cherenkov peak, while gate 2 probed the scintillation component. Of course, some fraction of the scintillation light contributed to the signals from gate 1 as well. However, the pure scintillation signals from the yellow filter side made it possible to determine that fraction with great precision. Knowing that fraction, the UV signals recorded in gate 1 could thus be corrected for scintillation contributions event by event on the basis of the gate 2 signals. In this way, pure digitized Cherenkov and scintillation signals were obtained from the crystal signals observed in the UV PMT.

The same information could also be extracted from the oscilloscope data. This allowed for more flexibility, since the gate boundaries could be optimized off-line. The data shown in the following were obtained with the latter method.

Much more information about the characteristics of the BGO crystal, and the separation of its signals into scintillation and Cherenkov components, is given in Ref. [6].

4. Experimental results for BGO

4.1. Calibration of the UV signal components

The UV Cherenkov and scintillation signals produced by the BGO crystal were calibrated separately with 50 GeV electrons.

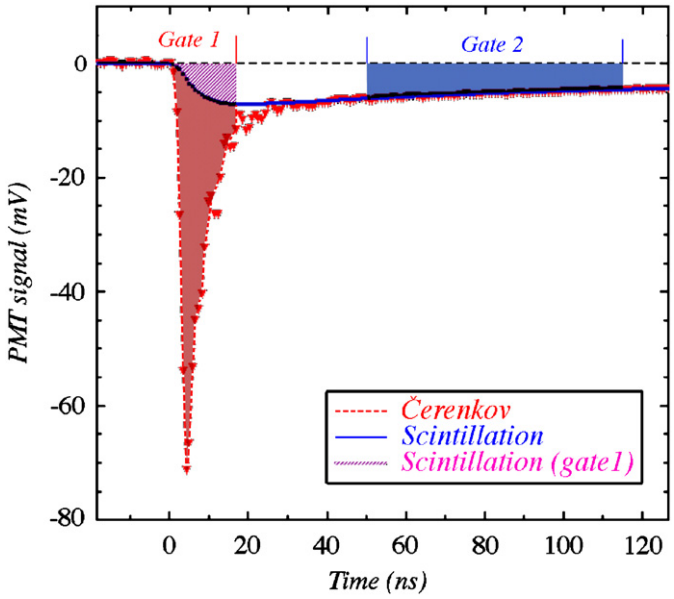

Fig. 6. The UV BGO signals were used to measure the relative contributions of scintillation light (gate 2) and Cherenkov light (gate 1). The oscilloscope sampled the time structure at intervals of 0.8 ns in this case. See text for details.

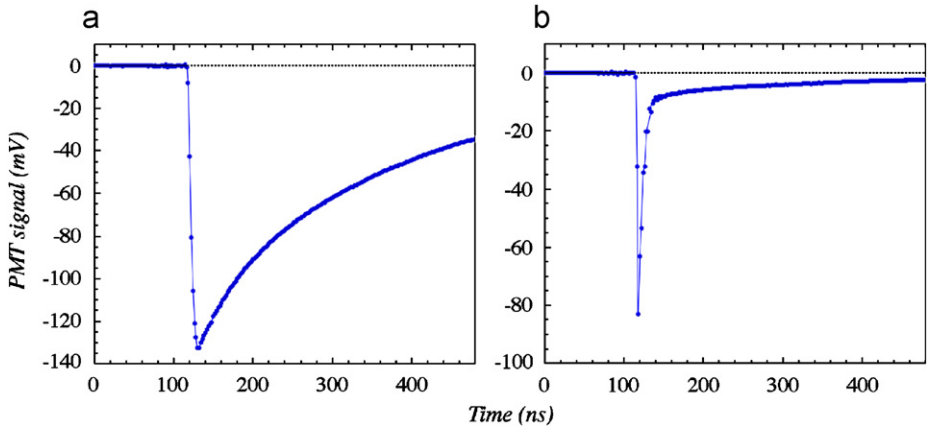

Fig. 5. The time structure of a typical shower signal measured in the BGO crystal equipped with a yellow filter (a), and with a UV filter (b). These signals were measured with a sampling oscilloscope, which took a sample every 2 ns in this case.

According to our Monte Carlo simulations, these electrons deposited, on average, 38.2 GeV in this crystal, with lateral (side) leakage being responsible for most of the lost energy.

Fig. 7 shows the results of this calibration, which was carried out for the oscilloscope signals. We defined gate 1 as the integrated charge collected during the first 16 ns of the pulse, while gate 2 integrated the charge from $t = 50-115$ ns. The gate 2 (pure scintillation) signal distribution is shown in Fig. 7a. The calibration constant, which converted the measured charge to energy units, was chosen such that this distribution centered around 38 GeV. Based on the oscilloscope signals from the yellow filter PMT, we concluded that the contribution of scintillation light to the gate 1 signal amounted to ~15% of the gate 2 signal. The gate 1 signals were thus corrected event by event for this contribution. Fig. 7b shows the gate 1 signal distribution before and after this correction. The calibration constant was chosen such that the latter distribution, which represents the Cherenkov component of the signals, also centered around 38 GeV.

Both the scintillation and the Cherenkov signal distributions had a relative width (σ/mean) of about 4.7%. This width was determined by fluctuations in the numbers of photoelectrons per unit deposited energy (which we will call the *light yield*), by fluctuations in shower leakage and by fluctuations in longitudinal shower development (which may affect the signal because of the effects of light attenuation). The numbers of photoelectrons were compatible for the two signals, and therefore a comparison of the widths of the two distributions did not make it possible to distinguish between these two sources of fluctuations. However, the distribution of the Cherenkov/scintillation (C/S) signal ratio, i.e., the event-by-event distribution of the ratio of the two components of the UV signals, provided more information in this respect, since it was less sensitive to the fluctuations that were unrelated to the light yield.

This distribution, shown in Fig. 8, is well described by a Gaussian function, with a relative width (σ/mean) of 6.0%. We conclude from these results that the Cherenkov light yield was at least 15 photoelectrons per GeV.

4.2. The pion signals

Now that the energy scale for the UV signals from the BGO crystal is set, we focus our attention on the signals from the 200 GeV π^+. The scintillation signal distribution for these particles is shown in Fig. 9.

The logarithmic scale is needed since a large fraction of the pions traversed the BGO crystal *without* starting a shower. The dominant mip peak is populated by these events. The nuclear interaction length of BGO is listed as 21.8 cm. However, this interaction length concerns protons, and the value for pions is typically up to 50% larger. An interaction length of 30 cm for pions would imply that ~45% of these particles traversed the 24 cm long crystal without undergoing a nuclear interaction. This is close to the observed fraction of events in the mip peak.

For this study, we were interested in the pions that started a shower in the BGO crystal and deposited a significant fraction of their energy in this crystal. We have selected events that deposited 20–40 GeV in the crystal (Fig. 9), where the energy

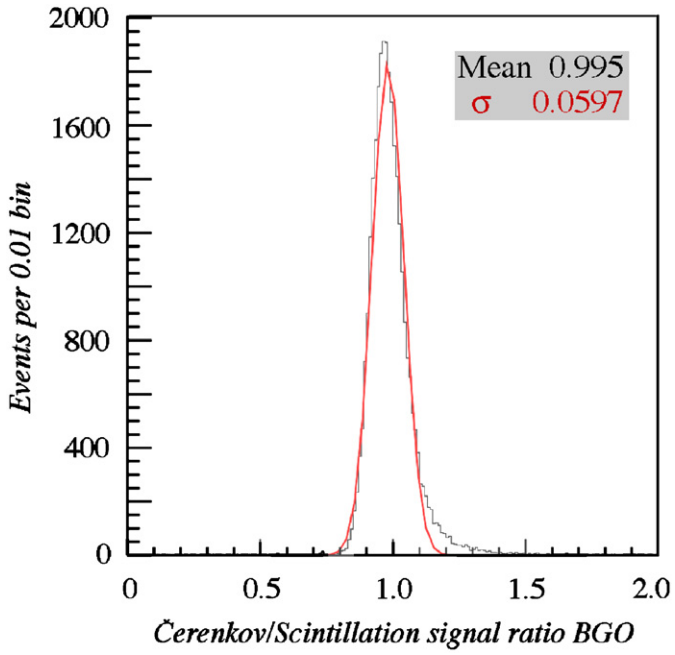

Fig. 8. Distribution of the Cherenkov/scintillation signal ratio for 50 GeV electrons showering in the BGO crystal.

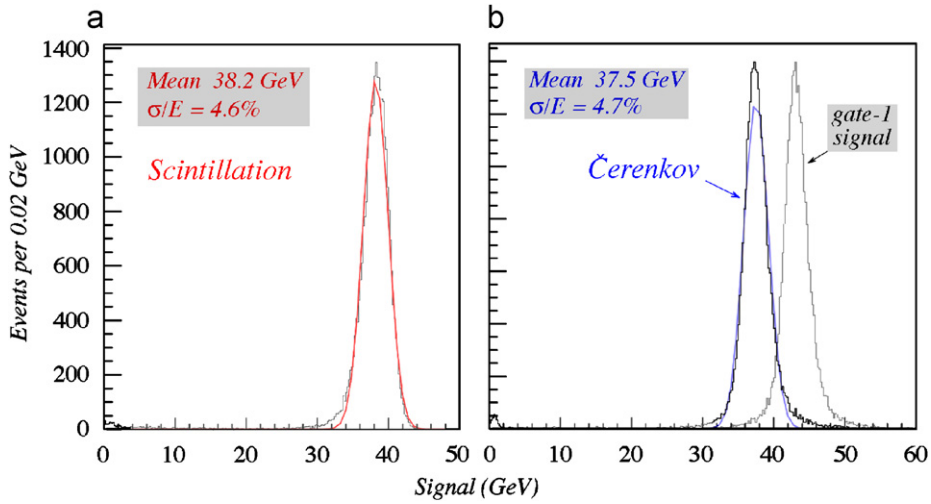

Fig. 7. Calibrated signal distributions for 50 GeV electrons in the BGO crystal. Shown are the distributions of the scintillation signals (a) and the Cherenkov signals before and after correcting for the contribution of scintillation light to the "prompt" component (b).

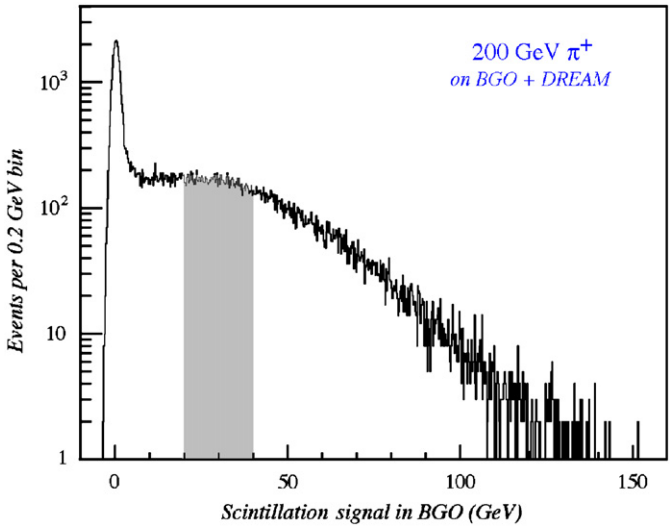

Fig. 9. Scintillation signal distribution in the BGO crystal, for 200 GeV π^+. The energy scale is derived from the electron calibration (Fig. 7a). Events in the shaded area were selected for further analysis.

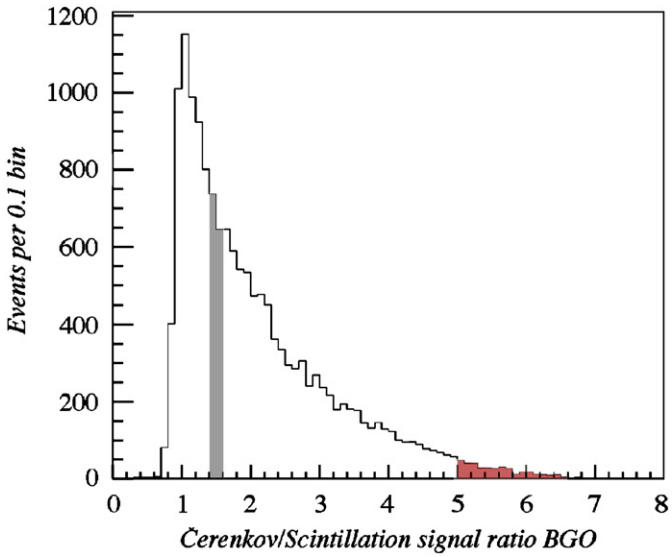

Fig. 10. Distribution of the Cherenkov/scintillation signal ratio for 200 GeV π^+ that started a shower in the BGO crystal and deposited 20–40 GeV in this crystal.

was determined from the UV scintillation signals, on the basis of the electron calibration described above. These events represented ~20% of the total, and ~40% of the non-mip events.

The distribution of the Cherenkov/scintillation signal ratio for the interacting pion events selected this way is shown in Fig. 10. This distribution looks very different from the equivalent one for electrons (Fig. 8). Many events exhibited Cherenkov signals that were considerably larger than the scintillation signals. The reasons for this phenomenon are discussed in detail in Section 4.4. Suffice it to say at this point that the underlying assumption of this study was that the C/S signal ratio is a measure of the π^0 production in the hadronic shower absorption process. In the next subsection, we investigate to what extent this ratio can be used to improve the hadronic performance of the calorimeter system as a whole, in the same way as we demonstrated this to be possible for the DREAM fiber calorimeter in stand-alone mode [3].

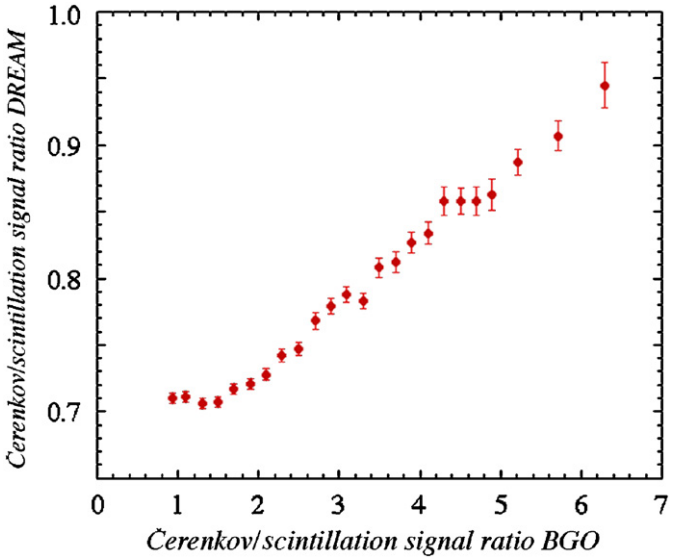

Fig. 11. The Cherenkov/scintillation signal ratio of the DREAM calorimeter, for 200 GeV π^+ starting a shower in the BGO crystal, as a function of the Cherenkov/scintillation signal ratio of the BGO signal.

4.3. ECAL/HCAL correlation

Because the BGO ECAL section of our calorimeter system was so small (less than 80% of the shower energy deposited by an electron was contained), large hadronic signals in the ECAL were likely to be caused by energetic π^0s produced in the early stages of the shower development. Therefore, it is reasonable to expect that hadronic events in which a considerable fraction of the energy was deposited in the BGO also exhibit substantial Cherenkov signals in the HCAL. In other words, one should expect a correlation between the C/S signal ratios in both sections of the calorimeter system. Fig. 11 shows that this correlation was indeed very strong, except for events that had relatively small C/S signal ratios.

Our analysis of the DREAM stand-alone data showed a strong correlation between the total hadronic calorimeter signal and the C/S signal ratio. This correlation formed the essence of the elimination of the effects of fluctuations in the em shower component, f_{em}, on the hadronic calorimeter performance [3]. Given the correlation observed in Fig. 11, it is therefore no surprise that in the present experiment the total signal observed in the HCAL was strongly correlated with the C/S signal ratio measured in the BGO ECAL.

This correlation is shown in Fig. 12a. The difference between the total signals for events with the largest and the smallest C/S signal ratios in the crystal ECAL was measured to be more than 50%. To put this result in perspective, we mention that this difference was measured to be less than 20% in a previous study, in which f_{em} was derived from the asymmetry between the signals from the two sides of an ECAL consisting of the $PbWO_4$ crystal matrix shown in Fig. 1, placed at an angle maximizing the difference between the relative contributions of Cherenkov light to both signals [5].

Interestingly, the fractional width of the signal distributions observed in the HCAL decreased as the events became more "electromagnetic". This is illustrated in Fig. 12b, which shows this width (σ_{rms}/mean) as a function of the C/S signal ratio in the crystal. It decreased from more than 30% for events with relatively small Cherenkov signals (i.e., low π^0 activity) to ~12% for events with the largest C/S signal ratios. It is well known that the hadronic energy resolution of calorimeters is strongly affected by fluctuations in invisible energy (e.g., nuclear binding energy

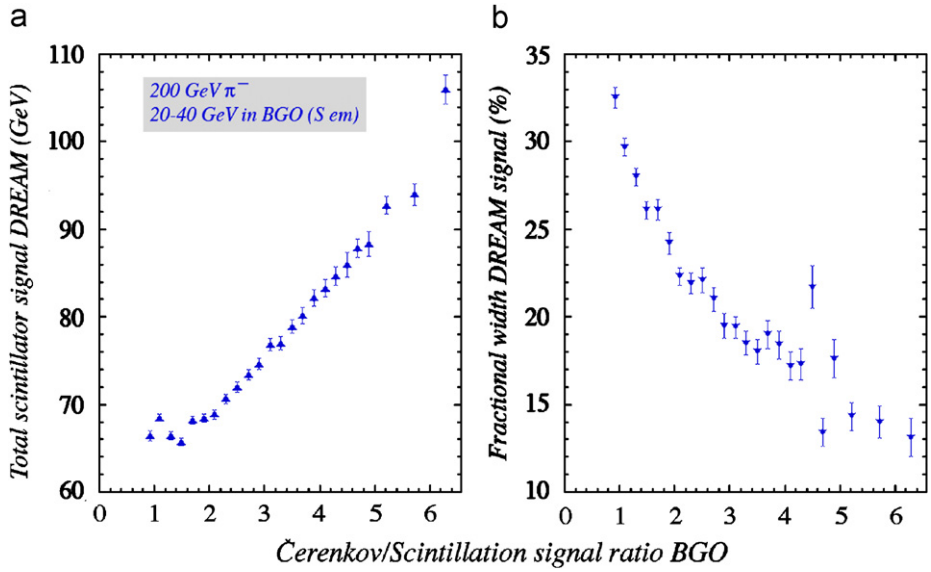

Fig. 12. The total scintillation signal (a) and the fractional width of the total scintillation signal distribution (b) in the DREAM calorimeter, for 200 GeV π^+ starting a shower in the BGO crystal, as a function of the Cherenkov/scintillation signal ratio of the BGO signal.

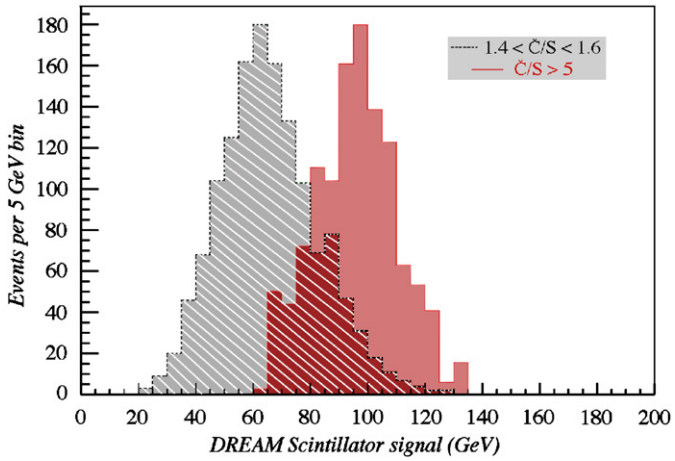

Fig. 13. The total scintillation signal distribution in the DREAM calorimeter, for 200 GeV π^+ starting a shower and depositing 20–40 GeV in the BGO crystal, for two different values of the Cherenkov/scintillation signal ratio of the UV BGO signals.

losses) [7]. Since such fluctuations only play a role in the non-em shower component, it is no surprise to see that the resolution improves for events in which a large fraction of the available energy was converted into em shower components, compared to events for which this fraction was smaller. This result thus confirms, once again, that the event selection on the basis of the Cherenkov/scintillation signal ratio in the BGO crystal was a good measure for f_{em}.

The results of this analysis are summarized in Fig. 13, which shows the distributions of the total scintillation signal measured in the fiber HCAL for subsets of events selected on the basis of the Cherenkov/scintillation signal ratio in the BGO ECAL. The signal distribution for the events with a large C/S signal ratio is considerably narrower and peaks at a larger value than the distribution for the events with a smaller C/S signal ratio.

4.4. Attenuation effects

There is one issue in the above analysis that remains to be addressed. The distribution of the C/S signal ratio in the BGO crystal looks very different for the pions (Fig. 10) than for the electrons with which the BGO signals were calibrated (Fig. 8). While the electron distribution is well described by a Gaussian with a mean value of 1.0, the pion distribution is highly asymmetric, and its mean value is 2.1. In this subsection, we investigate possible reasons for this difference.

Contrary to the electron showers, where most of the light was produced in the first half of the crystal, the light in pion-induced showers was, on average, produced much closer to the UV PMT that generated the signals we used for this analysis. Therefore, one might suspect that differences in light attenuation for the Cherenkov and scintillation components are responsible for the observed effects. In order to assess this possibility, we also took data with the BGO crystal rotated by 90°, i.e., oriented perpendicular to the beam line. Electrons of 50 GeV were sent into the crystal, which was moved in steps of 1 cm. In this way, the response of the two PMTs was measured over the full length of the crystal.

The oscilloscope data collected from these measurements were analyzed in the same way as described previously for the combined ECAL/HCAL data. The UV signals were separated in two parts, covering the "prompt" Cherenkov peak and the scintillation tail, respectively. The contribution of scintillation light to the "prompt" signals was determined on the basis of the time structure of the pure scintillation signals from the PMT behind the yellow filter.

The results of these measurements are summarized in Fig. 14. This figure shows that, while the overall signal in the UV PMT decreases as a function of the distance the light had to travel (Fig. 14a), the Cherenkov/scintillation signal ratio did not change much over the length of the crystal (Fig. 14b). A few comments are in order.

- The C/S signal ratio was somewhat smaller in these measurements than in the longitudinal geometry (Fig. 8), because of the different acceptance of the (directional) Cherenkov light in the crystal.
- The decrease of the total signal as a function of the distance was not only a consequence of light attenuation, but also of the tapered geometry of the crystal. As the distance to the UV PMT increased, the thickness of the crystal, and thus the amount of

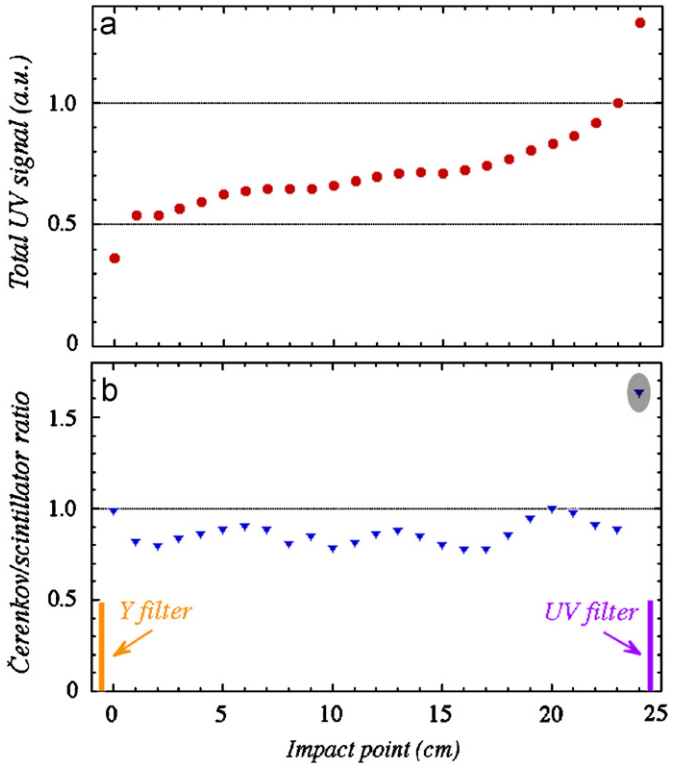

Fig. 14. The total UV BGO signal (a) and the ratio of the Cherenkov and scintillation components of that signal (b) as a function of the distance from the light production region to the PMT where it is detected. Data for 50 GeV electrons traversing the crystal perpendicularly.

light produced in it by the showering electrons, decreased (Fig. 3). The separate effects of attenuation and geometry on the crystal signals have been studied in detail in another paper [6].

Apparently, differences in light attenuation were thus not responsible for the different characteristics of the C/S distributions observed for pions and electrons. However, Fig. 14b does provide an important indication for the possible cause. The C/S ratio of the signals measured in the point closest to the UV PMT were anomalously high, more than a factor of 2 above average. This is due to the fact that in that case some of the shower particles traversed the glass window of the PMT and/or the filter and generated Cherenkov light (but no scintillation light) in that process. The filter/PMT combination thus served as an additional source of Cherenkov light, whenever charged relativistic shower particles traversed it.

This phenomenon could also very well explain the differences observed between the electron and pion signals. Especially when the pions produce an energetic π^0 in the last 10 cm of the BGO crystal, the filter/window may be located right at the shower maximum of the em showers through which this π^0 is being absorbed, resulting in substantial additional Cherenkov signals. Since this mechanism contributes exclusively to the Cherenkov signal, it would also explain why C/S signal ratios larger than those for electron showers were observed.

5. Experimental results for $PbWO_4$

Even though the $PbWO_4$ signals contain a substantially larger fraction of Cherenkov light than those from BGO (~15% at room temperature [8], vs. $\ll$1%), event-by-event information on the Cherenkov/scintillation ratio is considerably harder to extract because [6]

(1) The scintillation light is predominantly blue. Therefore, filtering is not an option to effectively distinguish the two components in this case.
(2) The decay of the $PbWO_4$ scintillation component is very fast, $\tau \lesssim 10$ ns at room temperature [8]. Contributions from the prompt Cherenkov component are thus much harder to disentangle.

Nevertheless, the excellent time resolution of our experimental setup made it also possible to distinguish between the prompt Cherenkov peak and the scintillation light in this case. This is illustrated in Fig. 15, which shows the average time structure of the $PbWO_4$ crystal signals recorded for the 200 GeV pions in the downstream photomultiplier tube (PMT B, see Fig. 2). The Cherenkov component is clearly visible and rather well resolved from the dominating scintillation component. The oscillating pattern superimposed on the trailing edge of this pulse is most likely the result of internal reflections of the directional light component in the crystal [6]. This explanation is corroborated by a comparison of the time structures in Figs. 18a and b.

In order to determine the Cherenkov fraction for individual events, we have used a method based on the fraction of the total signal that was recorded in the first 6.4 ns, $f(6.4)$. The larger this fraction, the larger the Cherenkov component of the signal [6]. This fraction (highlighted in Fig. 15) amounted typically to ~17%. As in the case of BGO, about half of the pions penetrated the $PbWO_4$ matrix without undergoing a nuclear interaction. The Cherenkov light generated by these pions went largely undetected, since the large index of refraction prevented it from exiting the crystal. As in the case of BGO, we were predominantly interested in the pions that started a shower in the crystal matrix and deposited a significant fraction of their energy in the crystal (Fig. 9).

Fig. 16 shows the distribution of $f(6.4)$ for these events. As expected, the average value is significantly larger as a result of these cuts. Assuming that $f(6.4)$ is a good measure for the production of Cherenkov light in individual events, we proceeded by investigating the characteristics of the signals in the hadronic fiber section in relation to the $f(6.4)$ value.

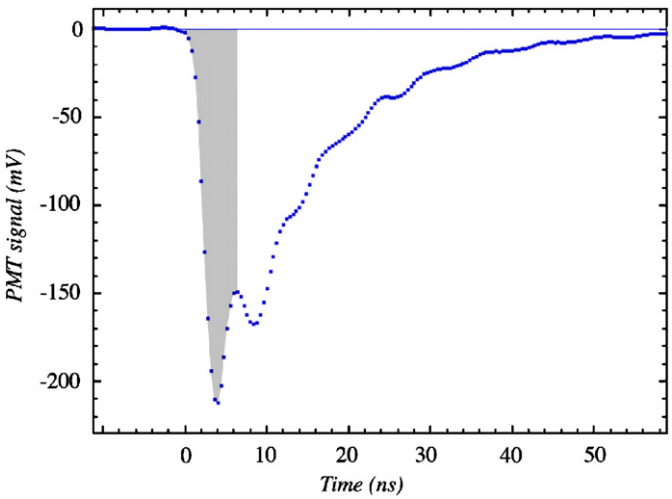

Fig. 15. Average time structure of the $PbWO_4$ signals recorded for 200 GeV π^+ in the downstream PMT of the $PbWO_4$ ECAL. The light collected during the first 6.4 ns (16 bins) is highlighted.

Fig. 17 shows the same phenomena as observed for BGO (Fig. 12). As $f(6.4)$ increases, the total (scintillator) signal observed in the hadronic section increases and the energy resolution of the signal distribution in the hadronic section improves. This is exactly what one would expect as a result of an increase of the (average) electromagnetic fraction of the events. We conclude that $f(6.4)$ is a good measure of the Cherenkov content of the $PbWO_4$ light, and thus of the em shower content. Other measures, such as the ones discussed in the previous section, confirmed that conclusion.

To underscore the fact that also the signals from the $PbWO_4$ ECAL can be used to determine the em fraction of the showers developing in this calorimeter system, we have selected two subsamples of events with different $f(6.4)$ values: $0.15<f(6.4)<0.17$ for subsample 1 and $0.35<f(6.4)<0.37$ for subsample 2. These subsamples are indicated by the highlighted regions in Fig. 16. Fig. 18 shows the average time structures (a and b) as well as the distributions of the total hadronic scintillation signal for these two subsamples (c).

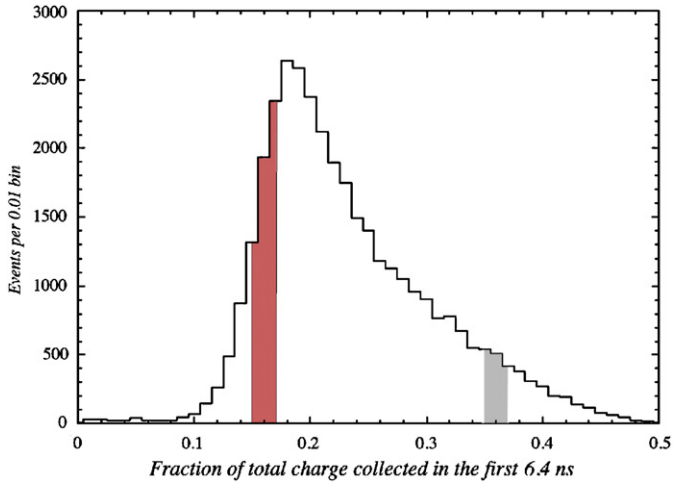

Fig. 16. Distribution of the fraction of the total signal collected during the first 6.4 ns, $f(6.4)$, for 200 GeV π^+ depositing 20–40 GeV in the $PbWO_4$ ECAL. The highlighted bands denote the subsamples used to make Fig. 18.

To put the results reported in this paper into perspective, it is interesting to make a comparison with similar results previously obtained with different methods. Fig. 19b shows the effects of selecting subsamples with a different em shower fraction (Fig. 19a), based on a direct measurement of the Cherenkov/scintillation signal ratio in the fiber calorimeter in stand-alone mode [3]. The results previously obtained with the $PbWO_4$ crystal matrix are shown in Figs. 19c and d. The latter analysis used the directionality of the Cherenkov light, and the asymmetry in the signals measured by two PMTs installed on opposite ends of the matrix (which was oriented at the Cherenkov angle of 63° with the beam direction) formed the basis of the measurement of the Cherenkov fraction for individual events [5].

The results obtained with the same $PbWO_4$ matrix in the experiments described in this paper are better than those shown in Figs. 19c and d. In addition, the new measurements, which are based on the time structure of the crystal signals, should in principle be applicable in a hermetic 4π detector, unlike the ones described in Ref. [5].

Yet, a comparison of the different results obtained with $PbWO_4$ and BGO indicates that the latter crystal is somewhat better suited for this type of application. Even though the BGO ECAL consisted of only *one* crystal, which did not even contain em showers at the 80% level, its capability to determine the Cherenkov fraction of the light generated by showering hadrons was better than for the much larger $PbWO_4$ matrix. The fact that the wavelength spectrum of the BGO scintillation light allowed an almost complete separation between the two different light components is of course responsible for this advantage.

6. Conclusions

We have shown that the signals from two types of crystals can be efficiently separated into Cherenkov and scintillation components. In the case of $PbWO_4$, this separation is accomplished on the basis of the time structure of the signals, while BGO offers

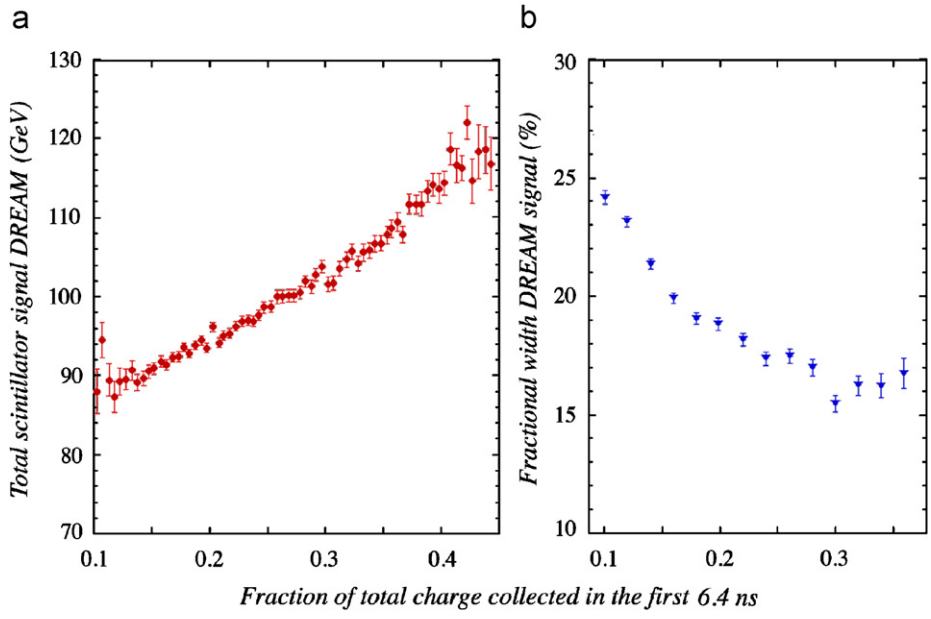

Fig. 17. The total scintillation signal (a) and the fractional width of the total scintillation signal distribution (b) in the DREAM calorimeter, for 200 GeV π^+ starting a shower in the $PbWO_4$ ECAL, as a function of the fraction of the total charge collected during the first 6.4 ns in the $PbWO_4$ signals.

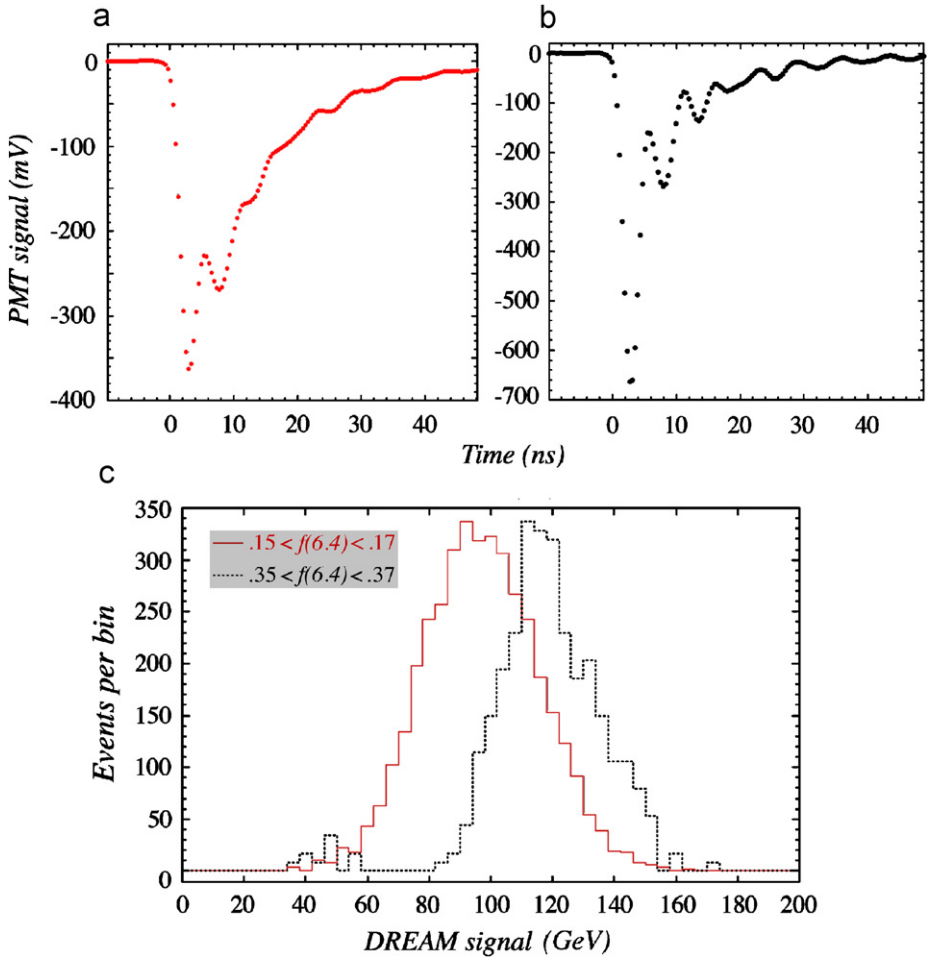

Fig. 18. Average time structure for events with $0.15<f(6.4)<0.17$ (a) and $0.35<f(6.4)<0.37$ (b), and the total scintillation signal distributions in the hadronic calorimeter section for both subsamples (c).

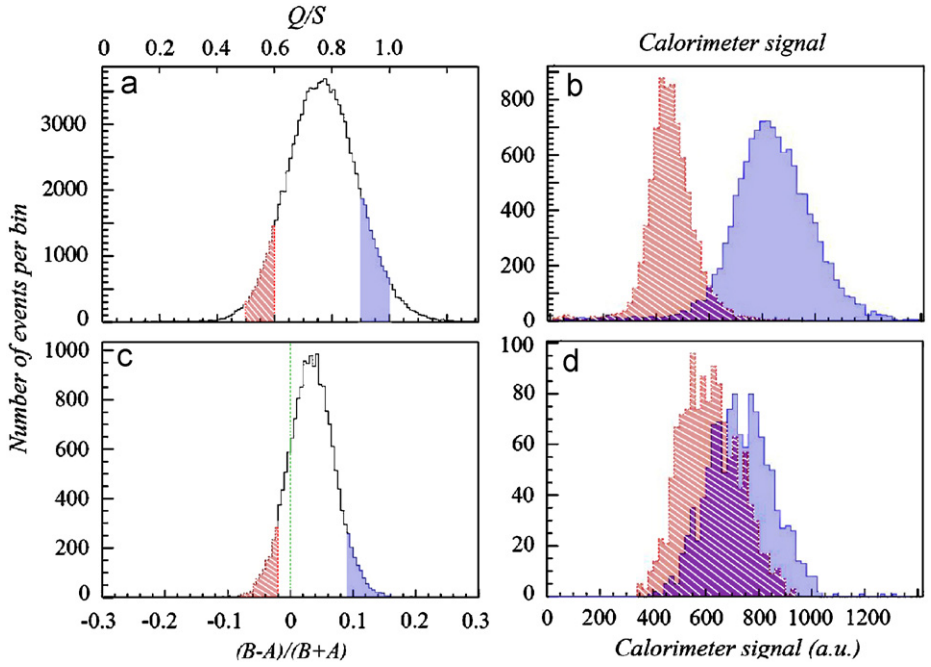

Fig. 19. Total hadronic signal distribution in the DREAM fiber calorimeter, for two event samples with a different electromagnetic fraction (b,d). The em fraction was determined on the basis of the ratio of the signals measured in the quartz and scintillating fibers (Q/S) of the calorimeter itself (a) [3] or from the directionality of the signals measured in a $PbWO_4$ crystal matrix installed upstream (c) [5].

in addition differences in the spectra of these components as a tool to achieve that goal. Our tests with the latter crystal indicate that the event-by-event determination of the Cherenkov component, and thus of the electromagnetic shower fraction in hadronic shower development, is of comparable quality as that achieved for the DREAM fiber calorimeter, where the two components were measured with two physically separate active media [3].

The experiments described in this paper primarily served to demonstrate the proof of principle of this technique. The crystals used in our setup, which did not even fully contain the electromagnetic showers used to calibrate their signals, were much too small for a serious quantitative assessment of the improvements in hadronic energy resolution and linearity that could be achieved, let alone for the detection of multiparticle events, which are essential for that purpose. Our next goal is therefore to assemble a BGO ECAL with the same lateral dimensions as the fiber module, which should enable us to make such an assessment.

Acknowledgments

We thank CERN for making particle beams of excellent quality available. This study was carried out with financial support of the United States Department of Energy, under Contract DE-FG02-07ER41495.

References

[1] R. Wigmans, et al., New J. Phys. 10 (2008) 025003.
[2] N. Akchurin, et al., Nucl. Instr. and Meth. A 536 (2005) 29.
[3] N. Akchurin, et al., Nucl. Instr. and Meth. A 537 (2005) 537.
[4] N. Akchurin, et al., Nucl. Instr. and Meth. A 533 (2004) 305.
[5] N. Akchurin, et al., Nucl. Instr. and Meth. A 584 (2008) 273.
[6] N. Akchurin, et al., Nucl. Instr. and Meth. A 595 (2008) 359.
[7] R. Wigmans, Calorimetry—energy measurement in particle physics, International Series of Monographs on Physics, vol. 107, Oxford University Press, Oxford, 2000.
[8] N. Akchurin, et al., Nucl. Instr. and Meth. A 593 (2008) 530.